Ion exchange purification of a silver nitrate electrolyte

Virolainen Sami, Holopainen Olli, Maliarik Mikhail, Sainio Tuomo

DOI: 10.1016/j.mineng.2018.12.020

Ion exchange purification of a silver nitrate electrolyte

Sami Virolainen[a, *], Olli Holopainen[a], Mikhail Maliarik[b], Tuomo Sainio[a]

[a]*Lappeenranta University of Technology, Laboratory of Separation Technology, P.O. Box 20, FI-53851 Lappeenranta, Finland*

[b]*Outotec Oyj, P.O. Box 475, SE-931 27, Skellefteå, Sweden*

**Corresponding author. Tel.: +358 50 4316756, E-mail address: Sami.Virolainen@lut.fi*

Declarations of interest: none

Abstract

A novel ion exchange process was studied to remove high concentration of Cu impurity from $AgNO_3$ electrolyte was studied. A suitable ion exchange resin was screened using laboratory scale experiments with a synthetic nitrate electrolyte solution of the following composition: 80.5–90.3 g/L Ag and 37.9–44.3 g/L Cu. Based on simulations with a developed mechanistic ion exchange model, a process scheme was constructed for the best resin, 2-(aminomethyl)pyridine functional chelating CuWRAM. The process was shown to be capable of producing 0.46 BV/h of a purified electrolyte solution containing >70 g/L Ag and <10 g/L Cu. Based on the simulations, roughly 10% of the Ag would be lost to eluate, but because the model overestimates Ag adsorption, the actual percentage is assumed to be lower as based on breakthrough experiments as the model overestimates the Ag adsorption.

Keywords

Silver; Electrolyte; Copper; Electrorefining; Ion exchange; Chelating resin; 2-(aminomethyl)pyridine

1. Introduction

A typical industrial Ag electrorefining process produces Ag cathodes of ≥99.99% purity from impure Ag anodes. During this process, dissolved impurities, such as Cu, accumulate in the electrolyte solution, which lowers the purity of the produced Ag cathode. When the Cu concentration in the electrolyte solution exceeds a certain level, *e.g.* 40–60 g/L, a bleed stream needs to be taken for impurity removal (Maliarik *et al.*, 2014; Aprahamian *et al.* 2016).

There are two main approaches to treat bleeds in industrial-scale Ag electrorefining processes: Cu precipitation using base metal salts (Aprahamian *et al.*, 2016) and Ag cementation (Maliarik *et al.*, 2014). The precipitation method is utilized by the Royal Canadian Mint (Aprahamian *et al.*, 2016) and based on the patents of Harris *et al.* (2008 and 2012). Cu precipitation is achieved by the constant removal of the HNO_3 vapors formed when $Cu(NO_3)_2$ hydrolyzes at a high temperature. The Cu yield in the precipitation process can be over 80% with very low amounts of co-precipitated Ag (0.01–0.1% reported in Aprahamian *et al.*, (2016)). Drawbacks includes issues caused by the acid vapors (requiring special safety, material, and chemical treatments) and the high energy consumption required for the elevated temperature (typically over 150 °C).

The cementation method utilized in the Ag electrorefining process by Outotec, which has been installed in 11 locations worldwide (Maliarik *et al.*, 2014). The Ag is cemented from the bleed solution using a reducing agent, such as Cu metal (Keleş, 2009). Because the cemented Ag is not pure enough to be a product, it is recycled back to the smelter (Maliarik *et al.*, 2014). Given that the yield is *e.g.* 99.2% (Keleş, 2009), an additional Ag trap is

54 needed for the raffinate because the Ag concentration is tens of mg/L. In addition, the use
55 of cementation increases the Ag inventory, and the consumption of fresh electrolytes and
56 chemicals is rather large. Patent literature on the precipitation purification (base metals
57 including Cu) of the $AgNO_3$ electrolyte also includes methods by Green (1971), Cai
58 (2006), Li *et al.* (2008), and Guo *et al.* (2016).

59 Table I. Research literature on $AgNO_3$ electrolyte purification methods. SBA = strong
60 anion exchanger, WBA = weak anion exchanger.

Method	**Target**	**Description**	**Reference**
Ion exchange	Pd	SBA resin VP-1P	Lebed *et al.* (2011)
Ion exchange	W 200–500 mg/L	WBA resin IRA-68	Natansohn and Czupryna (1983)
Ion exchange	Cu 1.9 g/L + others	Chelating resin with amino carboxyl functionality	Dowa Mining Co., Ltd., Japan (1985)
Ion exchange	Pd	Amidoxime polyacrylonitrile functional resin	Wu *et al.* (2012)
Solvent extraction	Cu, Ni, Co, Zn	Cation exchange reagents	Shiga (1978)
Solvent extraction	Hg(II)	SBA reagent Aliquat 336 complexed by a polyaminocarboxylic acid	Cote *et al.* (1992)
Nanofiltration	Bi, Sb, Pb, Cu, Te, Pd	Functional membrane rejects multivalent ions	Liu *et al.* (2012)

61 In addition to the industrial processes, the $AgNO_3$ electrolyte has been purified using ion
62 exchange, solvent extraction, and nanofiltration (Table I), among which ion exchange
63 seems to be the most popular. These processes remove several metals, and the separation
64 materials used cover the range from strong to weak anion and cation exchangers, and
65 chelating functionalities. Notably, none of these processes remove such high
66 concentrations of Cu as is the target in this study.

The literature contains general references to the ion exchange removal of Cu from electrolytes, mainly Co, and chelating resins have primarily been used for this purpose (Chen *et al.*, 2009; Wen *et al.*, 2010; Kotze, 2012; Yahorava *et al.*, 2013). Two of these processes are industrial, namely those used in the Kakanda tailings project (Democratic Republic of the Congo) and the Bulong Nickel Co refinery (Kalgoorlie, Western Australia) (Kotze, 2012). The Kakanda project's feed solution contained 40–100 mg/L Cu and 55 g/L Co, which indicates that the chelating exchangers are also selective enough for $AgNO_3$ electrolyte purification. The high Cu/Ag selectivity of the iminodiacetic functional groups was reported in the fundamental ion exchange studies of Samczynski (2006).

However, there is a research gap in understanding how ion exchange can be applied in the removal of Cu from the $AgNO_3$ electrolyte. The only available reference is a patent by Dowa Mining Co., Ltd., Japan (1985), in which the reported Cu concentration was much lower (1.9 g/L) than in the present case and typical industrial processes (*ca.* 40 g/L). Moreover, the patent describes neither the scientific background of the process nor the related chemistry.

In this study direct selective removal of Cu from the $AgNO_3$ electrolyte using a novel ion exchange process was investigated. In such a purification, the product would be a pure $AgNO_3$ solution that could be recycled directly back to the electrorefining tanks without further treatment. The target concentrations for the purified electrolyte were set at >70 g/L for Ag and <10 g/L for Cu, and the feed typically contained 84 g/L of Ag and 41 g/L of Cu. Implementing this unit process in Ag electrorefining processes will likely make them more techno-economically efficient. This study contains also development of mechanistic

model for the separation process, which enhances the understanding and predictability of the kind ion exchange processes.

2. Experimental

2.1 Chemicals and resins

The following chemicals were used in the experiments: NaOH (VWR Chemicals, purity >98%), H_2SO_4 (Merck, 95–97%), NH_4OH-solution (Merck, 25%), $AgNO_3$ (ThermoFisher, >99%), and $Cu(NO_3)_2 \cdot 2.5H_2O$ (ThermoFisher, 98%). The electrolyte solution was prepared by dissolving $AgNO_3$ and $Cu(NO_3)_2 \cdot 2.5H_2O$ in purified water, and the pH was adjusted with HNO_3. According to the analyses, the composition of the solution used was 80.5–90.3 g/L Ag and 37.9–44.3 g/L Cu, and the pH was 3.5. The industrial Ag electrolytes also contain also other impurities. However, for this developmental stage, the decision was made to focus exclusively on Cu/Ag selectivity and to use synthetic feed solutions instead of authentic ones.

Five different ion exchangers were used: Purolite C104 (The Purolite Company), Dowex 50x8 (The Dow Chemical Company), Lewatit TP207 (Lenntech), Dowex M4195 (The Dow Chemical Company), and CuWRAM (Purity Systems Inc., currently CuSelect by Johnson Matthey). These include chelating resins and conventional weak and strong cation exchangers (Table II). Before the experiments, the resins were washed with 1 M NaOH, H_2O, and 1 M H_2SO_4 and then converted to their desired ionic forms using these chemicals. For CuWRAM 1 M NH_4OH was used instead of NaOH because NaOH breaks its polyaminesilicate structure.

111 Table II. Resins compared for ion exchange purification of $AgNO_3$ electrolyte.

Resin	Structure	Functional group	Resin type	Ionic form
Purolite C104	Macroporous polyacrylic	-COOH	Weak cation	Base
Dowex 50x8	PS-DVB gel	$-SO_3$	Strong cation	Base
Dowex M4195	Macroporous PS-DVB	Bispicolylamine	Chelating	Acid
Lewatit TP207	Macroporous PS-DVB	Iminodiacetic acid	Chelating	Acid
CuWRAM	Polyamine silicate	2-(aminomethyl)pyridine	Chelating	Acid

112 For ion exchange resins, exothermic degradation reactions are possible under highly
113 oxidizing conditions, and Cu can act as a catalyst in these reactions (Purolite Ion Exchange,
114 2003). Thus, before starting the column experiments, the possible occurrence of these
115 reactions was studied in safe laboratory experiments. Each resin was mixed in a beaker
116 with the used electrolyte. Temperature was measured, and the formation of gases due to
117 the reactions was visually monitored. Overall, no oxidation reactions were observed.

118 *2.2 Column experiments*

119 All experiments were done in glass columns (YMC Europe GMBH), in which the fixed
120 bed was constructed from the resins. The volume of the resin bed for each experiment was
121 123.7 mL (d = 15 mm, h = 700 mm), and the temperature was 40 °C.

122 The loading stage in resin comparison experiments lasted for 2–3 BV, during which the
123 samples were collected at a rate of one per minute (40–60 loading samples from each run).
124 The flow rate was 3.0 BV/h. After the loading stage, the bed was rinsed with water to
125 remove the feed solution from its void fraction. The adsorbed metals were then removed
126 from the bed by eluting it with 6–10 BV of 1 M HNO_3 (flow rate 3.0 BV/h). For the first

six bed volumes samples were collected at a rate of 1.7 min/sample. After that, samples were taken at 30 min intervals.

The metal concentrations (Ag and Cu) of the samples were analyzed using ICP-MS (Agilent 7900). The samples had a $1{:}10^6$ dilution ratio with 1wt.-% HNO_3. The loading of each metal as a function of the feed volume was calculated by using the following equation to numerically integrate the breakthrough data:

$$\frac{m_{\text{ads}}}{V_{\text{bed}}} = \sum_i \left(c_0 - \frac{1}{2}\left(c_i + c_{i-1}\right)\left(V_i - V_{i-1}\right)\right) - \varepsilon c_0 \tag{1}$$

where

c_0	initial concentration, g/L
c_i	concentration at temporal point i, g/L
V_i	cumulative volume (in bed volumes) fed at temporal point i, -
ε	void fraction of the resin bed, -
V_{bed}	volume of the resin bed, L

3. Theory

Fig. 1 gives the structure of the 2-(aminomethyl)pyridine functional CuWRAM resin. The polyamine network containing the pyridine groups is attached to silica backbone. The sorption mechanism is based on the binding of cations to the lone electron pairs in the nitrogen atoms. As electroneutrality in the resin must be conserved, an anion, in this case nitrate, is also sorbed. Therefore, the mechanism can be considered to be sorption of electrolytes. In this study, acidic elution is used, which means that the metal ions bound to the resin are exchanged with the protons. The reactions for the loading and elution steps are presented in Eqs. 2 and 3, respectively. The overbars denote the resin phase, and M denotes either Cu or Ag.

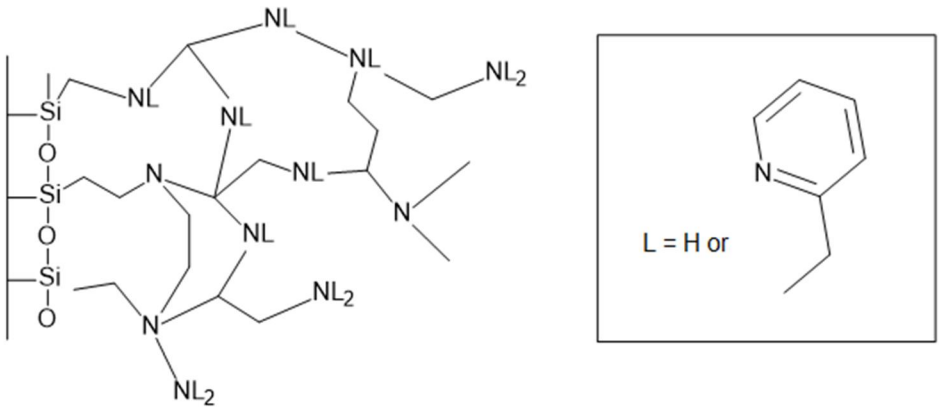

Figure 1. Structure of the 2-(aminomethyl)pyridine functional CuWRAM resin, drawn according to Laatikainen *et al.* (2010).

$$M^{n+} + nNO_3^- + \overline{:NR} \rightleftarrows \overline{(NO_3)_nM:NR} \quad (2)$$

$$\overline{(NO_3)_nM:NR} + nH^+ \rightleftarrows \overline{NO_3H:NR} + M^{n+} \quad (3)$$

Because of the system's complexity, as it includes several components and high concentrations, a simple stoichiometric ion exchange model based on mass action law could not explain the data with an accuracy sufficient for process simulations. Therefore, the sorption equilibrium was modeled using the non-ideal competitive adsorption isotherm equation (NICA, Kinniburgh *et al.*, 1999), which is derived from the competitive Langmuir equation with some additional parameters. Also, an additional term describing the physisorption of the metal nitrates was added (Eq. 2). In this equation, the affinity constant κ describes the median binding ability of component *i* to site *k*:

$$q_i = q_{tot} \sum_{k=1}^{S} \omega_k \frac{h_{i,k}}{h_{H,k}} \frac{\left(\kappa_{i,k} c_j\right)^{h_{i,k}} \left[\sum_j \left(\kappa_{j,k} c_j\right)^{h_{j,k}}\right]^{p_k - 1}}{1 + \left[\sum_j \left(\kappa_{j,k} c_j\right)^{h_{j,k}}\right]^{p_k}} A_{i,NO_3} c_i c_{NO_3} \quad (i, j = 1 \ldots N; k = 1 \ldots \mathrm{S}) \qquad (4)$$

where

	q_i	adsorption capacity for component i	mol/kg
	q_{tot}	proton capacity	mol/kg
	κ	affinity constant	L/mol
	c	concentration	mol/L
	S	number of different adsorption site types	-
	h	stoichiometry parameter	-
	H	proton	-
	ω_k	fraction of site k	-
	p	heterogeneity parameter	-
	$A_{i,NO3}$	parameter for metal nitrate adsorption	$L^2/(mol \cdot kg)$

Because only one adsorption site type was considered in this study, $S = 1$ and $\omega_k = 1$. Each individual adsorption site was assumed to have similar properties, and the parameter p describing the heterogeneity of site k was therefore 1. The maximum proton binding capacity, h_H, is assumed to equal the total amount of functional sites.

The mass balance equation for a differential volume element in the adsorption column was given as

$$\frac{\partial c_i}{\partial t} + v \frac{\partial c_i}{\partial x} + \left(\frac{1 - \varepsilon_b}{\varepsilon_b}\right) \frac{\partial \overline{q_i}}{\partial t} - D_{ax} \frac{\partial^2 c_i}{\partial x^2} = 0 \qquad (5)$$

where

	v	interstitial velocity	m/s
	x	axial coordinate	m
	ε_b	porosity of the resin bed	-
	D_{ax}	axial dispersion coefficient	m^2/s

In these simulations, ε_b is regarded as a constant (ε_b = 0.43). The axial dispersion was neglected (D_{ax} = 0), and dispersion was generated numerically due to the low order spatial discretization algorithm. The volume-average loading, $\bar{q}$, was calculated by using the linear driving force model, in which the mass transfer flux was calculated according to Eq. (4). Concentration layer approximation was used to calculate the LDF mass transfer coefficient (Eq. (5), Yao and Tien, 1993):

$$\frac{\partial \overline{q_i}}{\partial t} = \frac{6}{d_s} k_{s,i} \left(q_i^* - \overline{q_i} \right) \tag{6}$$

$$k_{s,i} = \frac{4 D_{s,i}}{d_s} \left(\frac{q_i^*}{\overline{q_i}} + \frac{1}{2} + \frac{\overline{q_i}}{q_i^*} \right) \tag{7}$$

where

$k_{s,i}$	mass transfer coefficient	m/s
$D_{s,i}$	diffusion coefficient in resin phase	m^2/s
d_s	diameter of resin particle	m

In Eqs. (5) to (7), an overbar denotes the volume-averaged concentrations in the resin phase, and an asterisk denotes surface concentrations.

Overall, there were four equilibrium model parameters (κ_i, h_i, $A_{i,NO3,}$ and $D_{s,i}$) to be fitted to each competing electrolyte in the system (HNO_3, $AgNO_3$, and $Cu(NO_3)_2$). The fitting was done visually against the collected dynamic adsorption column breakthrough data (see Section 4.4.). This is because the data were rather noisy and a strictly numerical minimization of the residuals would have led to a worse fit for certain regions of the breakthrough profiles where accuracy is critical for the process performance calculations. The resin specific properties needed for these calculations were taken from Sirola *et al.*

(2008) and Laatikainen *et al.* (2010): q_{tot} = 2.8 mol/kg, solids content (density) of swollen resin = 0.69 kg/L.

4. Results and discussion

4.1 Choice of resin

Breakthrough and elution curves were determined for five cation exchange resins to find the most efficient one for $AgNO_3$ electrolyte purification. The dynamic Cu and Ag capacities are given for each resin in Table III.

Table III. Dynamic Cu and Ag sorption capacities of the resins studied for the removal of Cu from the $AgNO_3$ electrolyte in a column.

Resin	q_{dyn}**(Cu), g/L$_{bed}$**	q_{dyn}**(Ag), g/L$_{bed}$**
Purolite C104	48.5	119
Dowex 50x8	21.0	115
Lewatit TP207	38.8	25.9
CuWRAM (acid)	18.6	0.485
CuWRAM (base)	12.9	0.808

Although with the CuWRAM chelating resin the adsorbed amounts of metals were low (Cu 18.6 g/L$_{bed}$ and Ag 0.485 g/L$_{bed}$), it had by far the best selectivity of the studied resins (Table III). Moreover, this resin's selectivity was to the right direction, meaning that it preferred Cu over Ag. After the bed was saturated with the metals, Cu was replaced Ag. This caused a high Ag peak (Fig. 2a) and led to the very low transfer of Ag to the eluent (Fig. 2b). Moreover, the elution behavior of the CuWRAM resins was favorable because the Cu eluted as a sharp peak without any significant tailing. Therefore, the CuWRAM resin was chosen as a viable candidate for electrolyte purification and for further

experimental and simulation studies. The resin was also tested in its base form (curves not shown), but, compared to its acid form, the adsorbed Cu amount was lower and the Ag amount was higher (Table III).

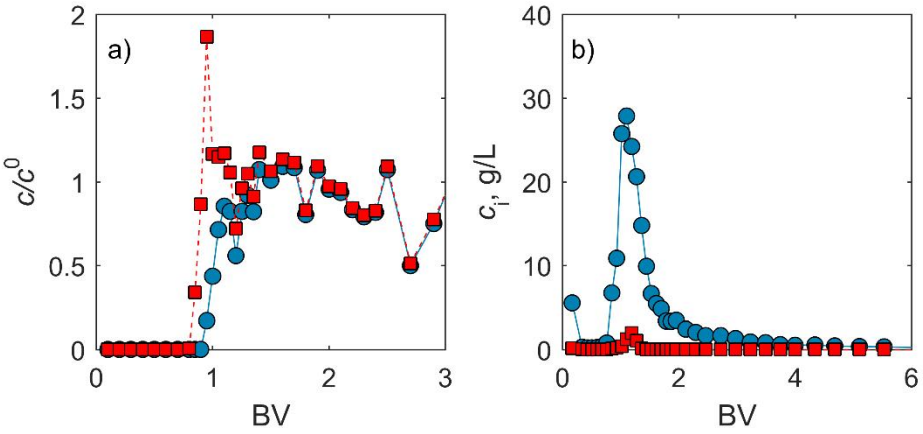

Figure 2. Column loading (a)) and elution (b)) curves of the 2-(aminomethyl)pyridine functional CuWRAM resin used for the removal of Cu from the $AgNO_3$ electrolyte. Symbols: circles Cu, squares Ag. Feed: 41.9 g/L Ag, 84.4 g/L Cu. *T* = 40 °C, Flow rate 3.0 BV/h.

Because the 2-(aminomethyl)pyridine functional CuWRAM resin is selective especially for Cu (Laatikainen *et al.*, 2010), the observed selectivity in the breakthrough experiments was expected. The dynamic Cu sorption capacity was also close to the maximum Cu sorption capacity (1 mmol/g or 26 g/L_{bed}) determined by Sirola *et al.* (2008) in sulfate solutions.

The weak cation exchanger Purolite C104 did not show the desired selectivity between Cu and Ag, and the strong cation exchanger Dowex 50x8 exhibited significantly higher sorption of Ag than Cu (Table III). With the latter, the separation could be done in a reversed order such that a solution containing Cu could be collected in the loading stage and a solution containing Ag in the elution stage, but a significant amount of Cu would be transferred to the eluent as well.

In general, cation exchangers prefer ions with higher charges and ions with smaller hydrated radii (Helfferich, 1995). Despite the higher charge of Cu^{2+}, the non-chelating cation exchangers used in this study (Purolite C104 and Dowex 50x8) preferred Ag^{+}. This is likely due to its smaller hydrated radius (Ag: 0.212 nm, Cu: 0.297 nm (Marcus, 1991)), which leads to both a higher charge density and a lower swelling pressure inside the resin particles. The speciation in the solution was calculated using the computer program MEDUSA (KTH Royal Institute of Technology, School of Chemical Engineering) to verify that the dominating species were Ag^{+} and Cu^{2+} and that no other cations existed in the soluble Ag area (E_h > 0.8 V).

For the chelating resin Lewatit TP207, no selectivity between Ag and Cu was observed during the loading stage (Table III). Iminodiacetic acid functional resins are selective for divalent heavy metals. Interestingly, the Cu/Ag selectivity observed during the breakthrough experiments was lower than that expected based on the literature (Inamuddin and Luqman, 2012; Samczynski, 2006), but the present case is also very extreme for an ion exchange process due to its high concentrations and oxidative conditions.

For the bispicolylamine functional chelating resin Dowex M4195, salts formed in the resin bed and clogged the flow through the column. Industrial scale operations using this resin were thus deemed unfeasible. The appearance of the precipitate suggested that it was $AgNO_3$, but Ag_2SO_4 would also be possible. Because the ion exchange capacity of the Dowex M4195 resin is significantly higher than that of the CuWRAM resin (Sirola *et al.*, 2008), the amount of acid liberated due to the Cu and Ag uptake is consequently higher, and this is the probable cause of the observed precipitate. Based on solubility calculations with MEDUSA, there is a significant decrease in the solubility of Ag in the pH range *ca.*

0.6–2.5 or when the sulfate concentration increases to 0.1 M and above. Therefore, the Dowex M4195 resin could be a feasible option with a different pretreatment.

4.2 Effect of the flow rate on purification performance

To study the possible non-ideal behavior of the ion exchange system in terms of dispersion, further column experiments were conducted using the CuWRAM resin and three distinct flow rates (3.0 BV/h, 6.5 BV/h, and 9.0 BV/h). The parameters of the ion exchange model described in Section 3 were also fit to the data. The results are shown in Table IV and Fig. 3.

Increasing the flow rate from 3.0 BV/h to 6.5 BV/h significantly decreased the dynamic capacities of both Cu and Ag (34% and 69%, respectively) (Table IV). However, the change from 6.5 BV/h to 9.0 BV/h had very little effect. While no experiments were done for higher flow rates, the purification would likely be sufficient even at flow rates over 10 BV/h.

In theory, the flow rate should not affect the dynamic capacities when the column is working ideally and the system is run until equilibrium, as was the case with the experiments in this study. Thus, a non-ideal flow phenomenon, such as flow maldistribution (Helfferich, 1995), has likely caused these decreased dynamic capacities.

Table IV. The effect of the flow rate on the dynamic sorption capacities of Cu and Ag using the CuWRAM resin for the removal of Cu from the $AgNO_3$ electrolyte.

	Experimental			*Simulated*		
Flow rate, BV/h	**q_{dyn}(Cu), g/(L bed)**	**q_{dyn}(Ag), g/(L bed)**	**Purity of Cu in eluent, %**	**q_{dyn}(Cu), g/(L bed)**	**q_{dyn}(Ag), g/(L bed)**	**Purity of Cu in eluent, %**
3.0	18.5	0.44	97.7	12.2	3.59	77.3
6.5	13.8	0.26	98.2	12.2	3.52	77.6
9.0	13.3	0.27	98.0	12.1	3.48	77.7

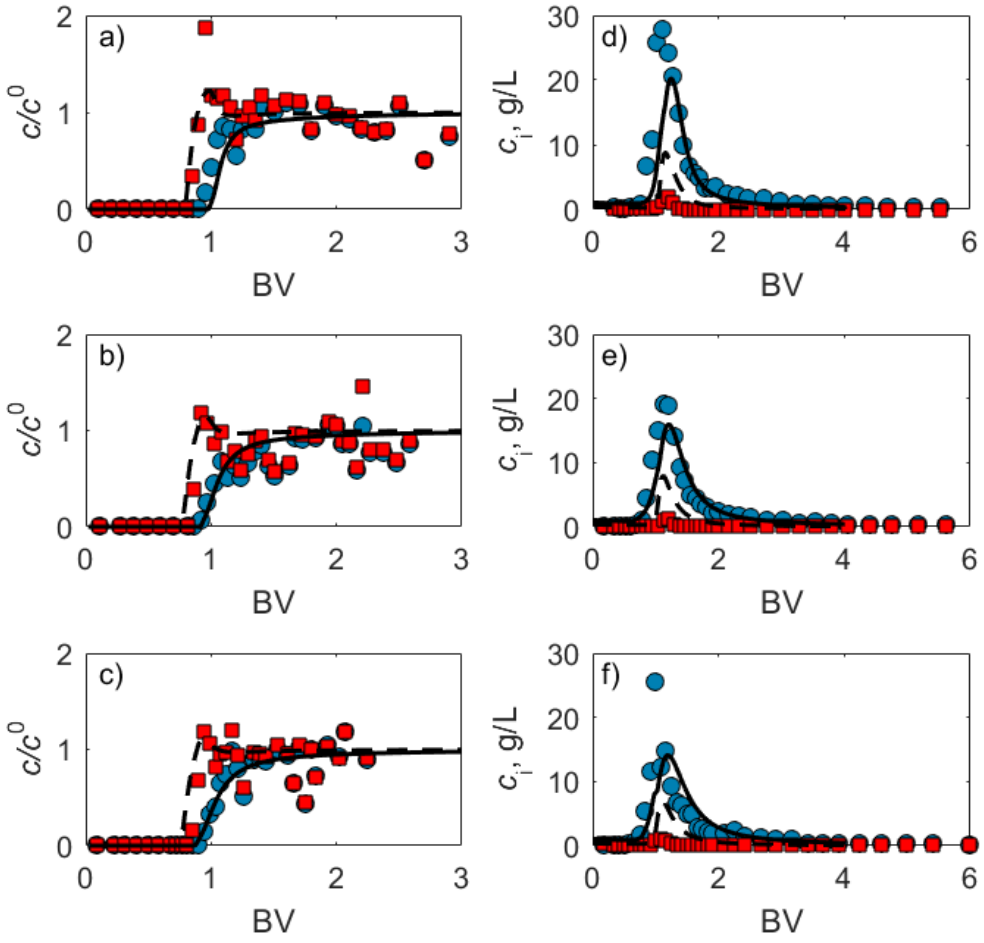

Figure 3. Experimental and simulated breakthrough curves for the loading (a), b), c)) and elution (d), e), f)) stages in the $AgNO_3$ electrolyte purification process. a) and d) 3.0 BV/h, b) and e) 6.5 BV/h, and c) and f) 9.0 BV/h. Symbols: circles Cu, squares Ag. Lines represent simulated curves. Feed: 84.4–88.2 g/L Ag, 40.4–43.2 g/L Cu. T = 40 °C.

4.3 *Water wash of the loaded resin*

After the loading step, the resin bed was washed with water to remove the feed electrolyte from its void fraction. However, the washing curves were not identical for Cu and Ag (Fig. 4), indicating the presence of an additional phenomenon besides the normal ion exchange. This was observed in several runs, which excludes the possibility of experimental or analytical error. It is likely that in the loading step some amount of Ag is attached to the resin by physisorption, and this Ag was then washed out from the resin with water. Because of this observation, the physisorption term was added to the non-ideal competitive adsorption isotherm used in the ion exchange model (Section 3).

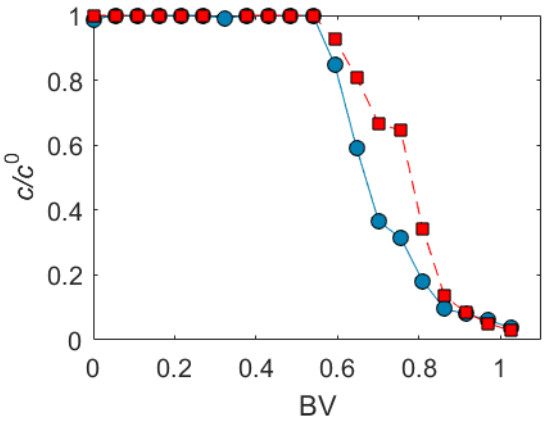

Figure 4. The water wash in ion exchange process for the removal of Cu from the $AgNO_3$ electrolyte. Flow rate 6.5 BV/h. Symbols: circles Cu, squares Ag. Feed: 84.2 g/L Ag, 41.7 g/L Cu. T = 40 °C.

4.4 *Evaluation of the ion exchange model*

The parameters of the chosen ion exchange model described in Section 3 were estimated by fitting the model results to the measured ones. This was done visually so that the simulated breakthrough curves would fit as well as possible to the experimental data for all three flow rates. The simulated curves are presented with the experimental data in Fig. 3.

311 The obtained parameters are given in Table V. The good selectivity of this resin for Cu
312 over Ag is also reflected in the equilibrium affinity parameters (log κ). In addition, HNO_3
313 has a strong affinity to the functional group, and this relatively high basicity has previously
314 been reported in the titration of the resin (Sirola *et al.*, 2008). HNO_3 and $AgNO_3$ are also
315 sorbed by the physisorption mechanism, although, as observed from the water washing
316 curves, $Cu(NO_3)_2$ is not (Fig. 4).

317 Table V. Fitted parameters for the ion exchange model used in $AgNO_3$ electrolyte
318 purification with the 2-(aminomethyl)pyridine functional CuWRAM resin.

	log κ	***h*, -**	**$A_{i,NO3}$, $L^2/(mol \cdot kg)$**	**$D_{s,i}$, m^2/s**
HNO_3	1.3	0.60	0.07	$8.00 \cdot 10^{-11}$
$AgNO_3$	0.0	0.30	0.07	$8.00 \cdot 10^{-10}$
$Cu(NO_3)_2$	1.7	0.33	0.00	$9.00 \cdot 10^{-11}$

319 Although the very high concentrations in the feed solution are challenging from a modeling
320 perspective, the simulated loading and elution curves (Fig. 3) fit the experimental data well.
321 The only major differences are in the Ag elution curves, as the eluted amounts are
322 significantly higher in the simulated observations than the experimental ones. This
323 phenomenon originates in the loading stage because the model predicts too high of a
324 loading for Ag. Thus, the equilibrium model parameters that simultaneously predict the
325 correct breakthrough points and equilibrium loadings could not be identified. It was
326 deemed more important to correctly predict the breakthrough points because this is a
327 critical operating parameter for the cyclic process outlined in Section 4.5.

328 The shapes of the all loading and elution curves are similar with the experimental data.
329 However, with 3.0 BV/h flow rate, it was not possible to describe the experimentally

observed Ag peak in the loading curve at around 0.9 BV (Fig. 3) without negatively affecting the fits of the other loading curves. While this system can possibly cause such a strong displacement during its dynamic column operations, it was experimentally observed only in a single point. Thus, experimental error cannot be excluded. With the 3.0 BV/h flow rate, the breakthrough in the simulated Cu curve occurred later than in the experimental Cu curve (Fig. 3).

The simulated breakthrough curves are similar for the different flow rates, with only slight difference in the shapes of the curves (Fig. 3). Dynamic adsorption capacities were calculated from the simulated curves (Table IV), and they were almost identical. This is the expected result because the experimentally observed non-ideal flow-phenomena were excluded from the model. This non-ideality presents a major modeling challenge. The experimentally determined dynamic capacities changed significantly between flow rates, and non-ideal phenomena are difficult to model. By using the same model parameters for each flow rate, the experimentally determined and simulated capacities deviate from each other. In this case, the slowest flow rate (3.0 BV/h) had the greatest deviation. In general, the simulated dynamic capacities for Cu were slightly lower than the experimental capacities and those for Ag were significantly higher. In other words, the simulation model underestimated the performance of the ion exchange process, especially in terms of the amount of Ag transferred to the eluent (Table IV).

Despite these issues, it was concluded that the simulation model was accurate enough to study the dynamic process for the purification of the $AgNO_3$ electrolyte because how the model's results are affected by its lack of a perfect fit with the Ag elution profile has been established.

4.5 Process design using dynamic simulations

Numerical simulations were used to test the feasibility of Ag electrolyte purification using an ion exchange process. The composition of the feed was 84 g/L Ag and 41 g/L Cu, and the process capacity was arbitrarily set to 1000 L of feed per 24 h. The product specifications were given as concentrations in the raffinate stream: $c_{Ag} \geq 70$ g/L for Ag and $c_{Cu} \leq 10$ g/L for Cu.

The flowsheet of this process is shown in Fig. 5. It operates batchwise, taking 1000 L of electrolyte bleed to the feed tank every 24 h, and contains an internal recycling stream to achieve a high Ag recovery yield. Methods to design single-column chromatographic or ion-exchange processes with internal recycling streams and even evaporators (Siitonen *et al.*, 2011; Hellstén *et al.*, 2012) do exist. However, they are not directly applicable here because this process requires a strong eluent, resulting in additional washing steps, and cannot be operated in a steady state. The following process sequence was chosen based on the experimental results discussed in Sections 4.1–4.3:

1. Water wash. After an ion exchange cycle, the HNO_3 solution is removed from the void fraction of the bed. Duration: 5 BV.
2. First loading step. The resin takes all the metals from the feed solution, and pure water is collected from the outlet. This is recycled to the water tank. Duration: 0.7 BV.
3. Second loading step. The actual product, a pure $AgNO_3$ electrolyte, is collected as the raffinate. The product can be recycled directly back to the electrorefining process. Duration: until the Cu achieves a value of 0.71, given as c/c^0.
4. Third loading step. To prevent the loss of yield during elution, the resin is fully loaded to displace as much Ag as possible. Duration: until a combined feed amount of 2 BV is achieved for the loading steps (2–4).
5. Water wash. The feed solution containing Ag and Cu is washed from the resin bed. Excess water is evaporated from this solution so that recycling it back to the feed tank will not reduce the feed concentrations. Duration: 1.5 BV.

6. Elution. Cu and traces of Ag are eluted from the resin with HNO_3. After this, the resin is in its acid form and ready for the next process cycle. This step yields an almost pure $Cu(NO_3)_2$ solution. Traces of valuable Ag may be trapped from this solution. Duration: 4 BV, full elution assumed.

The size of the bed needed to process 1000 L in under 24 h was 127 L. The simulations were completed for feed flow rates of 3.0, 6.5, and 9.0 BV/h. In each simulation, the flow rate was 30 BV/h during the washing stage and 10 BV/h during elution, and these values were chosen based on the previous experiments. The simulation was conducted using the cyclic process described above. After each cycle, new amounts and compositions for the feed tanks were calculated and then used for the next cycle.

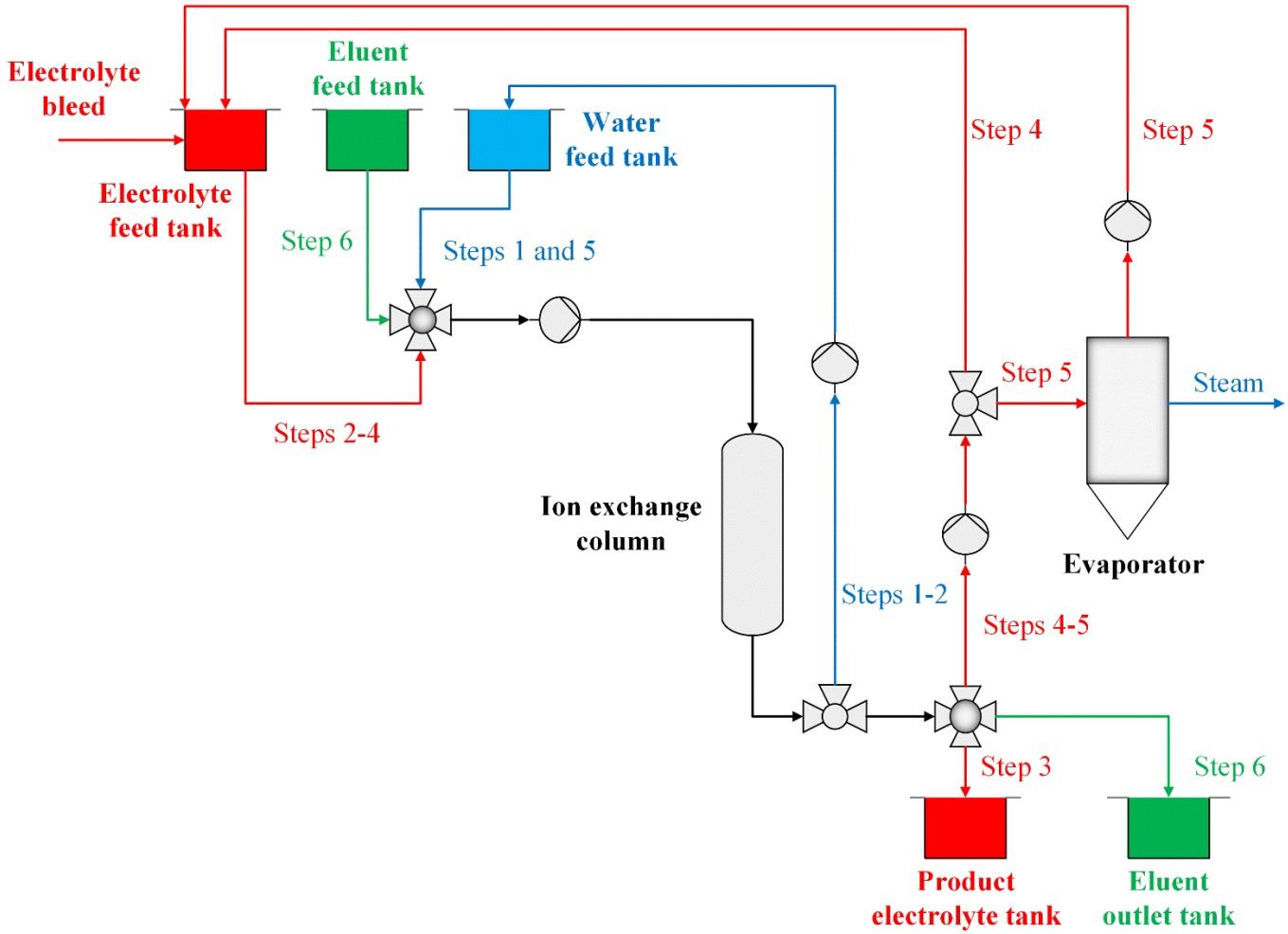

Figure 5. Flowsheet of the suggested process for $AgNO_3$ electrolyte purification using an ion exchange process.

In the simulated process, successive cycles increased the Ag concentration and decreased the Cu concentration (Fig. 6). The water wash solution was recycled back to feed tank (Fig. 5), causing both concentrations to decrease. In the suggested process, a high Cu concentration is needed to efficiently remove the adsorbed Ag from the resin. Therefore, the evaporation step for the dilute washing water is necessary (step 5), and this increases the Ag concentration.

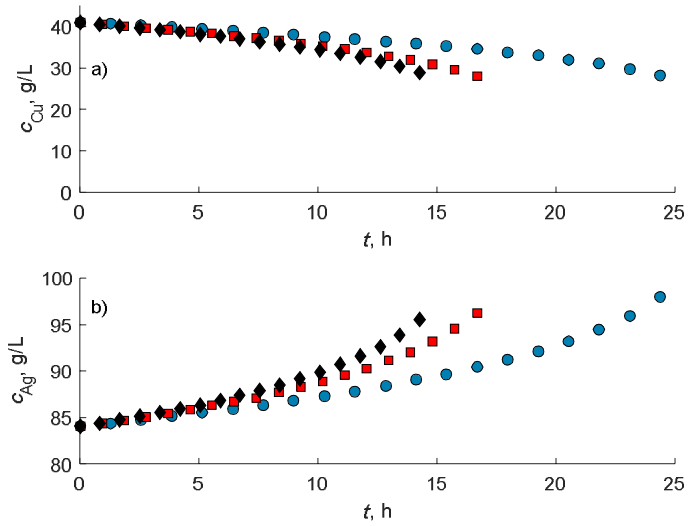

Figure 6. Simulated concentrations of the feed electrolyte in $AgNO_3$ electrolyte purification using an ion exchange process. a) Cu, b) Ag. Symbols: circles 3.0 BV/h, squares 6.5 BV/h, triangles 9.0 BV/h. Feed: 84 g/L Ag, 41 g/L Cu.

The amount of treated electrolyte solution per time unit depends on the feed flow rate (Fig. 7a). Using the 3.0 BV/h flow rate, 1000 L of the electrolyte solution is treated in 23.1 h. Using the 9.0 BV/h flow rate, it takes only 14.3 h. The dependence of the collected eluent amount as a function of the flow rate gave similar results of faster growing amounts (Fig. 7b). Although the amount is high (*ca.* 9000 L), eluent recycling was not considered in this

study. Hence, a much lower eluent consumption could be achieved in reality. The simulated Cu and Ag concentrations in the eluate were 1.1–1.2 g/L and 3.7–3.9 g/L, respectively.

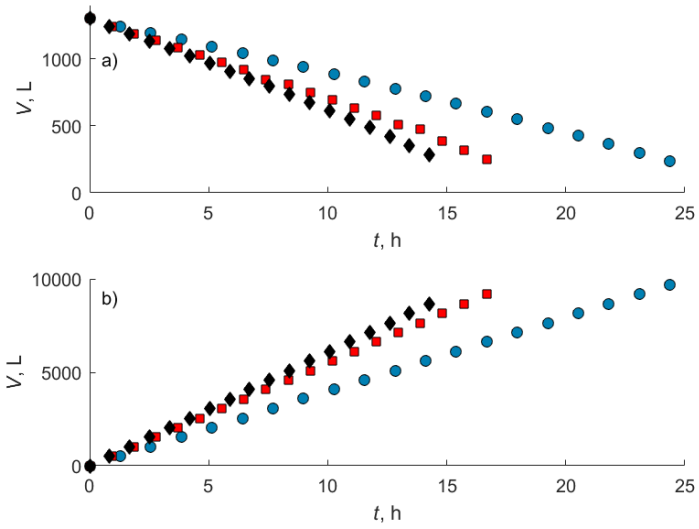

Figure 7. Simulated volumes of a) the feed electrolyte and b) the eluent outlet tanks in $AgNO_3$ electrolyte purification using an ion exchange process. Symbols for the feed flow rates: circles 3.0 BV/h, squares 6.5 BV/h, triangles 9.0 BV/h. Feed: 84 g/L Ag, 41 g/L Cu.

More metals are removed per time unit when the flow rate is increased, but the difference is not very large, especially when increasing the rate from 6.5 to 9.0 BV/h (Fig. 8). After treating 1000 L of the electrolyte solution, 78.9% of the Cu was removed with the 9.0 BV/h flow rate and 92.2% with the 3.0 BV/h flow rate. The amount of Ag lost to the eluent is higher than the set limit (10%) for each flow rate (Fig. 8). Given that the simulation model overestimates this loss heavily, it would likely be a small percentage in reality. In the breakthrough experiments, the amount of Ag transferred to the eluent was so low (Table IV) that an Ag free eluent seems possible (<5 mg/L Ag), which would avoid the need for an Ag trap.

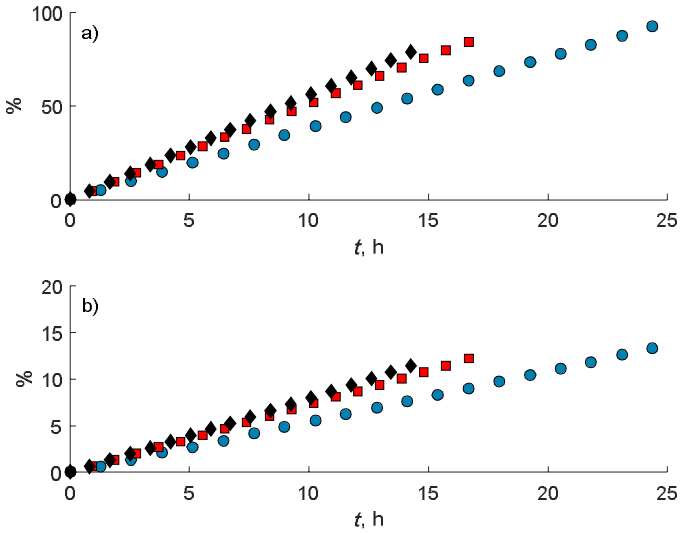

Figure 8. Simulated amounts of removed a) Cu and b) Ag in $AgNO_3$ electrolyte purification using an ion exchange process. Symbols: circles 3.0 BV/h, squares 6.5 BV/h, triangles 9.0 BV/h. Feed: 84 g/L Ag, 41 g/L Cu.

During the first few cycles, the quality of the Ag electrolyte product deteriorated slightly. But, due to the changing composition of the feed (Fig. 6), Ag concentration then increased and Cu concentration slowly decreased (Fig. 9). Each flow rate achieved the set goals (Ag >70 g/L and Cu <10 g/L) except for 9.0 BV/h, which gave a Cu concentration above 11 g/L. Compared to the others, the 3.0 BV/h flow rate gave also the highest Ag concentration in the product.

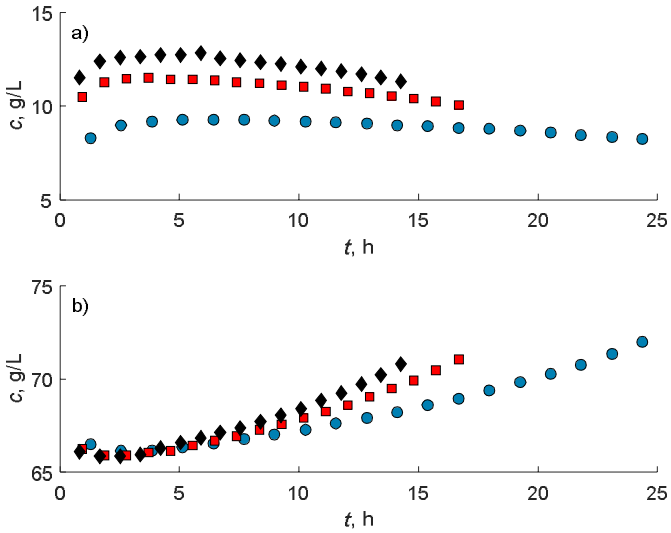

Figure 9. Simulated concentrations of a) Cu and b) Ag in the product of $AgNO_3$ electrolyte purification using an ion exchange process. Symbols: circles 3.0 BV/h, squares 6.5 BV/h, triangles 9.0 BV/h. Feed: 84 g/L Ag, 41 g/L Cu.

5. Conclusions

An ion exchange process for removing Cu impurities from the $AgNO_3$ electrolyte was designed. The 2-(aminomethyl)pyridine functional chelating resin CuWRAM was evaluated as the best option for separation, largely due to its excellent Cu/Ag selectivity. A mechanistic model was constructed to describe the separation system, and it was used to design an ion exchange process capable of purifying 1000 L of the electrolyte solution (84 g/L Ag and 41 g/L Cu) within one day. The suggested process contains six steps: three loading steps, from which one of them the pure $AgNO_3$ electrolyte product is taken, two water washing steps, and an elution step. Evaporation should be used for the solution coming from the second washing step to maintain a high Cu concentration in the feed tank.

Using a 3.0 BV/h feet flow rate, the purification of 1000 L of the electrolyte solution in a single column with a 127 L resin bed is completed in 24.3 h. However, with a 9.0 BV/h

feed flow rate, the purification takes only 14.3 h. Over 78% of the Cu (initial concentration 41 g/L) is removed with the 9.0 BV/h flow rate, and over 92% is removed with the 3.0 BV/h flow rate. The estimated Ag losses were tolerable at over 10%, but this amount was heavily overestimated in the simulations compared to the breakthrough experiments. The concentrations in the product electrolyte were typically under 10 g/L for Cu and over 70 g/L for Ag (initial 84 g/L), which is a good result. Notably, this solution can be recycled directly back to the Ag electrorefining process.

References

Aprahamian, V., Tangen, M., Harris, G.B., White, C.W., 2016. Royal Canadian Mint silver electrorefining bleed treatment, in: IMPC 2016: XXVIII International Mineral Processing Congress Proceedings. Presented at the IMPC 2016: XXVIII International Mineral Processing Congress, Canadian Institute of Mining, Metallurgy and Petroleum, Quebec City, Canada.

Dowa Mining Co., Ltd., 1985. Purification of silver electrorefining solutions. JP60050193A.

Cai, L., 2006. Method for purifying electrolyte for silver electroplating. CN1884623A.

Chen, A., Qiu, G., Zhao, Z., Sun, P., Yu, R., 2009. Removal of copper from nickel anode electrolyte through ion exchange. Transactions of Nonferrous Metals Society of China 19 (1), 253–258. https://doi.org/10.1016/S1003-6326(08)60261-7

Cote, G., Lizama, H., Esteban, S., Bauer, D., 1992. Extraction of mercury(II) complexes of various polyaminocarboxylic acids with a liquid anion exchanger. Application to the purification of electrolytic solutions of silver nitrate. J. Chem. Res., Synop. 150–151.

Green, G.R., 1971, Method of purifying aqueous silver nitrate solutions. US3554883A.

Guo, J., Zheng, Q., Gu, J., Ling, F., Wu, X., 2016. Preparation of high-purity silver by electrolysis of silver nitrate. CN105297074A.

Harris, B., White, C., Aprahamian, V., 2012. Method for recovering nitric acid and purifying silver nitrate electrolyte. US8282903B2.

Harris, B., White, C., Aprahamian, V., 2008. Method for recovering nitric acid and purifying silver nitrate electrolyte. WO2009000072A1.

Helfferich, F., 1995. Ion Exchange. Dover Publications, Inc.

Hellstén, S., Siitonen, J., Mänttäri, M., Sainio, T., Steady state recycling chromatography with an integrated solvent removal unit - Separation of glucose and galactose, J. Chromatogr. A., 1251(2012), 122-133. https://doi.org/10.1016/j.chroma.2012.06.047

Inamuddin, Luqman, M. (eds.), 2012. Ion Exchange Technology I, Springer + Business Media B.V. Doi: 10.1007/978-94-007-1700-8

Keleş, O., 2009. An optimization study on the cementation of silver with copper in nitrate solutions by Taguchi design. Hydrometall. 95, 333–336. https://doi.org/10.1016/j.hydromet.2008.07.006

Kinniburgh, D.G., van Riemsdijk, H., Koopal, L.K., Borkovec, M., Benedetti, M.F., Avena, M.J., 1999. Ion binding to natural organic matter: competition, heterogeneity, stoichiometry and thermodynamic consistency, Colloids Surf. A 151, 147–166. https://doi.org/10.1016/S0927-7757(98)00637-2

Kotze, M.H., 2012. What are the major roles of ion exchange in hydrometallurgy?. International Conference on Ion Exchange (IEX 2012), SCI, Cambridge, UK, September 18–21 (2012).

Laatikainen, K., Lahtinen, M., Laatikainen, M., Paatero, E., 2010. Copper removal by chelating adsorption in solution purification of hydrometallurgical zinc production. Hydrometall. 104, 14–19. https://doi.org/10.1016/j.hydromet.2010.04.005

Lebed, A.B., Makovskaya, O.Y., Skorokhodov, V.I., Naboichenko, S.S., Mal'tsev, G.I., 2011. Choice of a sorbent for selective extraction of palladium from silver refining electrolytes. Khim. Interesakh Ustoich. Razvit. 19, 535–540.

Li, Y., Liu, Q., Liu, J., 2008. Method for purifying Ag electrolyte during high-purity Ag production. CN101113526A.

Liu, W., Xie, Z., Yang, Y., Cao, Y., Cao, Y., 2012. Purification method of silver electrolyte by nanofiltration. CN102560536A.

Maliarik, M., Johansson, K.-A., Ögren, B., Berg, G., Johansson, C.-D., Lindh, R., Ludvigsson, G.M., 2014. High current density electrorefining process: technology, equipment, automation and Outotec's silver refinery plants, in: Proceedings of the 7th International Symposium Hydrometallurgy 2014. Presented at the Hydrometallurgy 2014, Canadian Institute of Mining, Metallurgy and Petroleum, Victoria, Canada.

Marcus, Y., 1991. Thermodynamics of solvation of ions. 5. Gibbs free energy of hydration at 298.15 K, J. Chem. Soc., Faraday Trans. 87, 2995–2999. Doi: 10.1039/FT9918702995

Natansohn, S., Czupryna, G., 1983. Separation of tungsten from silver nitrate electrolyte. Trans. Am. Inst. Min., Metall., Pet. Eng., Soc. Min. Eng. AIME 274, 1937–1940.

Purolite Ion Exchange, 2003. Risks of explosions when using ion exchange resins, Purolite International SRL.

Samczynski, Z., 2006. Ion exchange behavior of selected elements on Chelex 100 resin. Solvent Extr. Ion Exch. 24, 781–794. https://doi.org/10.1080/07366290600846174

Shiga, S., 1978. Purification of silver-containing solution formed during silver electrorefining. JP53067619A.

Siitonen, J., Sainio, T., Kaspereit, M., 2011. Theoretical analysis of steady state recycling chromatography with solvent removal, Sep. Purif. Technol. 78, 21–32. https://doi.org/10.1016/j.seppur.2011.01.013

Sirola, K., Laatikainen, M., Lahtinen, M., Paatero, E., 2008. Removal of copper and nickel from concentrated $ZnSO_4$ solutions with silica-supported chelating adsorbents. Sep. Purif. Technol. 64, 88–100. https://doi.org/10.1016/j.seppur.2008.08.001.

Wen, J.-J., Zhang, Q.-X., Zhang, G.-Q., Cao, Z.-Y., 2010. Deep removal of copper from cobalt sulfate electrolyte by ion-exchange. Transactions of Nonferrous Metals Society of China, 20 (8), 1534–1540. ISSN 1003-6326, http://dx.doi.org/10.1016/S1003-6326(09)60334-4

Wu, J., Yang, T., Liu, W., Xie, X., Zhang, D., Li, J., 2012. Method for separating palladium from silver electrolyte. CN102329959A.

Yahorava, V., Kotze, M., Auerswald, D., 2013. Evaluation of different adsorbents for copper removal from cobalt electrolyte. The Southern African Institute of Mining and Metallurgy, Base Metals Conference 2013.

Yao, C., Tien, C., 1993. Approximations of uptake rate of spherical adsorbent pellets and their application to batch adsorption calculations. Chem. Eng. Sci. 48, 187–198. https://doi.org/10.1016/0009-2509(93)80295-2